Building Extraction and Rubble Mapping for City Port-au-Prince Post-2010 Earthquake with GeoEye-1 Imagery and Lidar Data

Ejaz Hussain, Serkan Ural, KyoHyouk Kim, Chiung-Shiuan Fu, and Jie Shan

Abstract

This paper uses GeoEye-1 imagery and airborne lidar (Light Detection and Ranging) data to map buildings and their rubble in Port-au-Prince caused by the Haiti earthquake on 12 January 2010. This is achieved by performing an object-based one-class-at-a-time land cover classification of the image and lidar data using spectral, textural and height information. Classification accuracy is about 87 percent overall, and approximately 80 percent for buildings and rubble. Comparison of manually-selected 200 actual damaged buildings within an area of two sq. km in the city center shows an accuracy of over 90 percent for building and rubble mapping. 3D building models for approximately 55,000 buildings covering an area of 30 sq. km over Port-au-Prince were generated. It is found that most of the damage is to the concrete and masonry structures in the well planned areas of the city and very little damage to the shelters and the temporary type houses with metal sheet roofs. The study demonstrates that fusing optical imagery and lidar data can effectively map the nature, severity, extent and damage patterns caused by earthquakes in densely populated urban areas like Port-au-Prince.

Introduction

On 12 January 2010 a magnitude 7.0 Mw severe earthquake occurred in Haiti with its epicenter near the town of Léogâne, approximately 25 kilometers west of Port-au-Prince. The main jolt was followed by about 59 aftershocks of minimum 4.5 Mw or greater as reported by USGS (USGS; **http://earthquake.usgs.gov/earthquakes/recenteqsww/Quakes/us2010rja6.php#summary**. This earthquake caused widespread damage to buildings in and around Port-au-Prince, including some landmark buildings such as the Presidential Palace, the National Assembly Building, Port-au-Prince Cathedral, and the Headquarters of the United Nations Stabilization Mission. This earthquake, though less in magnitude as compared to historic Haiti earthquakes, is recorded as one of the most destructive in the history due to the number of human fatalities. The Haitian Government reported about 217,000 to 230,000 people as dead, 300,000 injured and 1,000,000 homeless (Wikipedia; **http://en.wikipedia.org/wiki/2010_Haiti_earthquake**). They also estimated that 250,000 residential and 30,000 commercial buildings were collapsed or severely damaged. Historic records show that earthquakes at such magnitude can cause moderate to very heavy damage even to earthquake-resistant structures (Ali *et al.*, 2008).

Remote sensing data are among the cost effective and accurate sources due to their wide coverage, timely availability and temporal frequency for mapping natural disasters spreading over broad areas. The importance and usefulness of remote sensing data have already been proven during many of the past natural disasters such as floods, forest fires and earthquakes all over the world (Turker and Sumer, 2008; Shan *et al.*, 2009). Information derived from remote sensing data greatly helps the authorities in rescue and relief efforts, damage assessment, and the planning of remedial measures to safeguard such events effectively. A range of satellite data sources are suitable for varying degrees of damage assessment including Landsat, SPOT, Ikonos, QuickBird, OrbView, GeoEye-1, and WorldView-2. Selection of a particular data source depends mainly upon the timely coverage, availability, spatial, spectral and temporal resolution, nature of analysis and finally the cost. In case of natural disasters, timely availability of remote sensing data is of prime importance for the rescue and relief efforts and mapping the extent, impact, and damage (van der Sande *et al.*, 2003).

Different methods can be used for mapping earthquake damage to buildings by incorporating the pre- and post-event remote sensing data in combination with elevation, lidar, and existing GIS data. Different change analysis techniques such as comparison of pre- and post-event thematic maps, post-event building thematic map and building vector data or field survey data can be used for quantitative assessment and categorical classification of the damage to buildings. However, these methods are dependent on the availability of relevant data. Most of the studies on previous earthquakes used pre- and post-event image data, and compared the classified thematic maps using different change detection techniques to estimate the damage to buildings (Rathje *et al.*, 2005; Gusella *et al.*, 2005; Yamazaki

Ejaz Hussain is with the National University of Science and Technology, Islamabad, Pakistan, and formerly with the School of Civil Engineering, Purdue University, West Lafayette, IN 47907.

KyoHyouk Kim and Jie Shan are with the School of Civil Engineering, Purdue University, West Lafayette, IN 47907 (jshan@ecn.purdue.edu).

Chiung-Shiuan Fu is with the Center for Remote Sensing, Agricultural & Biological Engineering, University of Florida, FL 32611.

Photogrammetric Engineering & Remote Sensing
Vol. 77, No. 10, October 2011, pp. 1011–1023.

0099-1112/11/7710–1011/$3.00/0

et al., 2005). Some studies used vector GIS data of the existing building boundaries and compared it to the buildings extracted from the post-event images to assess the damage. In one of the studies, Turker and Sumer (2008) used shadow as an indicator to map undamaged buildings from post-event images, and then compared the results with the pre-event building boundaries to estimate the damage. Turker and Cetinkaya (2005) used digital terrain model (DTM) generated from pre- and post-event aerial photos and compared height to estimate building damage. Generally, accurate and categorical building damage estimation requires some kind of pre-event data, such as high resolution images or building footprints. However, in the case of the Haiti earthquake, no pre-event high resolution images, DTM, digital surface model (DSM), or vector GIS data of buildings were immediately available for comparison and assessing building damage.

Immediately after the earthquake, disaster management agencies started rushing to Haiti to provide relief and rescue to the affected people. However, the absence of accurate and up-to-date local geospatial information was a major impediment to prepare and support their plans. Therefore, to meet the emerging need on geospatial data to expedite and accelerate the relief efforts, the UN (United Nations) and other relief agencies requested volunteers to collect and process geospatial data at the emergency footings. As a result, there have been numerous efforts by international agencies on remote sensing and field data acquisition. In parallel, the International Charter-Space and Major Disasters was also activated. It is a body that facilitates the provision of spaceborne and other geospatial data from archived, current and future acquisition to its members (Stryker and Jones, 2009). The provision of data through the Charter is free of charge. This centralized system of data collection and distribution works very efficiently and ensures provision of both pre- and post-event data to the research teams, experts, and relief and rescue organizations operating in the affected areas. Another major contribution by means of remote sensing and other geographic data distribution was from USGS Hazards Data Distribution System (HDDS). HDDS immediately started providing data to volunteer organizations, relief agencies, research groups, and the general public. All over the world, many institutions and universities volunteered for data processing and extraction of useful information from these data that can help the concerned agencies for planning and execution of rescue and relief operations.

This study is motivated by the importance of quick and accurate damage information considering its usefulness for concerned agencies to target earthquake affected areas and also estimate the economic losses and quantum of rubble. We use GeoEye-1 imagery and airborne lidar data over Port-au-Prince to perform object-based land-cover classification to assess how post-earthquake image and elevation data help mapping buildings and rubble. Building footprints obtained as a result of image classification are later processed for geometric and topological integrity and regularity. Regularized building footprints are used to generate 3D building models for better visualization of standing and partially damaged buildings. Similarly, the resultant rubble class is used to map its spatial distribution and estimate its quantities. The rest of the paper first describes the data we used in this study, the complexity of the problems, and an overview assessment on the earthquake damages. A land-cover classification strategy of one-class-at-a-time is presented as the first step of the solution. The resultant building class is then undergone simplification, regularization, topological enforcement, and 3D visualization. Similarly, the rubble class is used to map its spatial distribution and estimate its quantum. Extensive discussions are devoted to the difficulties encountered, their solutions, evaluation of the results, and the capabilities and limitations of remote sensing data in earthquake damage assessment.

Port-au-Prince Urban Area and Damage Overview

Data

The study area is about 30 sq. km urban area of Port-au-Prince. It mainly covers the city, especially the city center, most populous and planned parts of the city. A true color (RGB) pan-sharpened GeoEye-1 image, with 0.5 m spatial resolution, acquired on the next day after the main earthquake was used for mapping land-cover, building damage, and rubble. This image was selected as the major data source due to its timely acquisition, spatial resolution, and coverage. The first lidar data acquisition over Port-au-Prince was on 21 and 22 January 2010 as a collaborative effort of ImageCat, Inc. and the Rochester Institute of Technology (RIT) under the support of the World Bank. A DTM and DSM of 1 meter resolution were created and made available. We created nDSM (normalized digital surface model) by subtracting the DTM from DSM to extract the heights of the ground objects for subsequent analysis.

In some cases, data acquired from different sources are associated with mis-registration problems having an offset of meters. Combined use of such data needs a precise geo-registration effort before any other processing. These efforts started with the processing of the GeoEye-1 scene. The image was initially not geographically referenced; therefore, roads and streets from the OpenStreetMaps (OSM) database extracted by Geofabrik (2010) were used as a reference map for geo-rectification. This data set had the most detailed roads and streets compared to the other available data options by that time. These data provided more flexibility to select suitable ground control points for geo-rectification. The GeoEye-1 image was re-registered with nDSM in order to have both datasets in the UTM (Universal Transverse Mercator) coordinate system and to use them together for further analysis.

Complexity and Distribution of Building Structures

Port-au-Prince is one of the highly complex and heterogeneous urban areas. Areas in the vicinity of the presidential palace seem to be of a planned development with a reasonably regular road and street network. Buildings include single story, multistory houses and apartments, hotels, and churches, mostly of concrete structure and organized within proper blocks. The rest of Port-au-Prince urban area does not appear to follow similar development and zoning criteria. It looks like there is no distinction between residential, commercial, and industrial areas; rather there is a mix of all types of buildings. As observed from GeoEye-1 image, building structures in Port-au-Prince includes concrete structures with flat roofs of varying heights and sizes, wooden or steel frame buildings with corrugated metal sheet roofs, and low height metal sheet shelters (shanty housing) with very small sized dwellings. The concrete-based buildings with wooden or steel frames appear to be a combination of residential, commercial, and industrial buildings. However, a huge number of shanty houses comprised of metal sheet roofs are found in every part of the city. These shanty housing areas are without any planned development. Some of these houses are so small in size that it is hard to visualize or categorize these as living houses, temporary shelters, or junk yards. Shelters in such slums are very dense, with almost no gap between the houses and on very narrow irregular streets; thus, it is hard to find any edges or house boundaries even on very high-resolution (0.5 m) imagery. Examples of different types of structures and patterns in Port-au-Prince are shown in Figure 1.

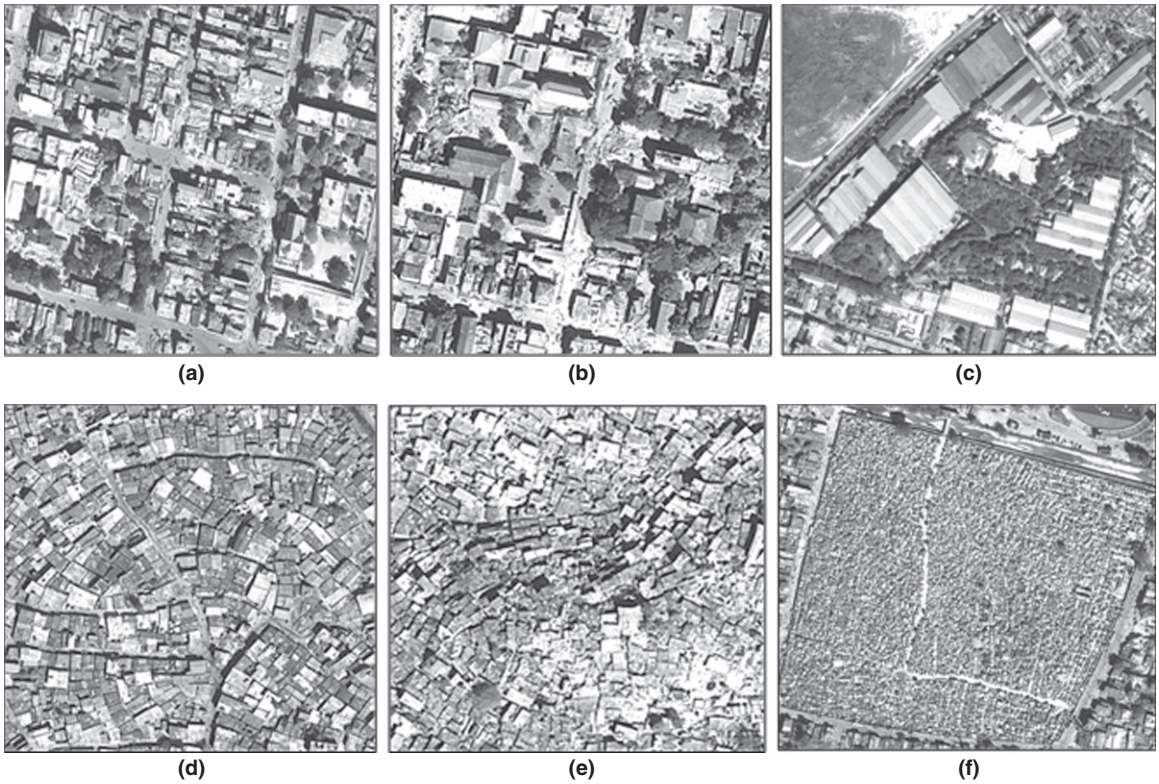

Figure 1. Different types of buildings in Port-au-Prince, Haiti: (a) and (b) mixture of concrete structures and wooden or steel framed structures with metal sheet roofs, (c) wooden or steel frame structures with metal sheet roofs, (d), (e), and (f) medium to very small size shanty housing with metal sheet roofs.

Observed Building Damage

Before applying any digital processing for classification, visual analysis of the imagery was carried out to explore and distinguish the nature, patterns, severity, and extent of the damage to different types of buildings caused by the earthquake. Such visualization of the damage was necessary to devise an image classification methodology for mapping the damage, rubble, and debris. Mainly three different types of building structures and damage patterns were observed in Port-au-Prince: concrete based structures with severe damage, steel and wooden frame buildings, and the shanty houses. Multiple collapse and damage conditions of different types of structures are enumerated below and shown in the image clips in Figure 2.

Concrete buildings (Figure 2a, 2b, and 2c):

- Complete collapse: broken roof and walls resulted entire building into rubble.
- Side or partition walls (infill wall) collapsed with intact or unbroken roofs.
- Roofs collapsed and caved in, walls partially damaged and some still intact; yielding a hollow look from top, i.e., shadow caused by standing walls partly cover rubble and debris.
- Partially collapsed walls and roofs, i.e., one side collapsed, other still intact; part of the building is down and partly intact.

Steel and wooden frame buildings with metal sheet roofs (Figure 2d):

- Mostly partial collapse, roofs still intact, building structure down with the collapse of side walls (bricks/concrete block walls)
- Partial damage/collapse, part of the roofs down, building deshaped and twisted (either wall or frame failure)
- Overall buildings intact, roofs partly broken, i.e., some of the roof sheets gone down, causing gaps and opening in roofs
- Walls still intact, but the metal sheet roof totally collapsed inside; giving a hollow look

Very low roof (Figure 2e):

- Hardly any visible damage or collapse; only roof sheets are missing at some places which may be due to the earthquake or already abandoned/unused structures

Land Cover Mapping

Approach

For land cover mapping with focus on the building class and the assessment of damage to the buildings caused by the earthquake, GeoEye-1 image integrated with nDSM is classified using object-based classification approach of Definiens Developer (**http://www.definiens.com**; Baatz and Schape, 2000). Object-based classification uses objects as classification unit rather than individual pixels. It is carried out in two steps: initially segmenting the image into homogeneous objects followed by classification. Classification is performed either using supervised nearest neighbor (NN) or fuzzy membership techniques (Walker and Blaschke, 2008).

Implemented in Definiens, the recently developed fractal net evolution approach (Baatz and Schape. 2000) uses both spectral and shape characteristics for segmentation. It is based on homogeneity criteria that include user-defined scale, color, and shape parameters. Their contributions to the segmentation process depend upon the user defined weights. Scale is an abstract value that determines the

Figure 2. (a) completely collapsed, (b) partially collapsed concrete buildings, (c), concrete buildings with intact walls and collapsed roofs, (d), steel or wooden frame structures with metal sheet roofing, side walls collapsed, partially damaged, twisted and de-shaped, and (e) shanty houses with broken roofs.

maximum possible change of heterogeneity, caused by fusing several objects, and controls the size of the resulting objects. Higher scale value allows merging of more objects to form larger ones, whereas lower scale value results in objects smaller in size. By carefully selecting the scale and shape parameters, an image is segmented into spatially contiguous, disjoint and homogeneous regions (Hay *et al.*, 2003). To maintain the geometry of the actual ground objects as closely as possible, object primitives can be achieved through a trial and error process using variable "scale" and "shape" parameters.

In the second stage, training sample objects are selected for every class of interest for nearest neighbor classification or knowledge based classification rules are formed using spectral, contextual and textural object features, and fuzzy membership functions (Benz *et al.*, 2004). A suitable selection and combination of features for every class with well defined fuzzy membership functions allow for a better classification and produce a very homogenous thematic map (Shackelford and Davis, 2003; Platt and Rapoza 2008; Congalton and Green, 2009). By setting the rules, classification can be performed collectively for all classes at once or sequentially for each class. Sequential classification helps to modify and update the rules at each run to achieve good classification results. The classification results depend on the input features and the resultant degree of membership value of a class. By using additional shape, context, and texture features, processing at object level, and with or without inclusion of ancillary data, object-based classification effectively handles very high resolution imagery (high spectral variability) and produces better classification results as compared to traditional pixel-based classifiers (Chen *et al.*, 2007; Shan and Hussain, 2009; Story and Congalton, 1986).

The GeoEye-1 image acquired on a day with clear sky over Port-au-Prince very effectively recorded the destructive effects of the earthquake on buildings and other infrastructure. Careful visual analysis of the image revealed that the nature of collapsed and damaged buildings, and resulting rubble and debris have no specific and distinguishable spectral response, shape, texture, and height information compared to other classes. Therefore, direct mapping of rubble or debris was not possible. Keeping this complex scenario in view, a method was pursued to include and sequentially classify all other possible land cover classes which possess some specific spectral, shape and height information. This approach led the process to where only damaged and collapsed buildings, and any other undefined objects were left unclassified. Finally, additional texture and context features were used to classify the rubble and debris from leftover unclassified objects. A flowchart showing the overall processing scheme is illustrated in Figure 3.

For better handling of the large dataset, fast segmentation, effective classification, and computational efficiency, a number of image tiles were created for both the image and the nDSM. Initially one representative image tile was used to perform classification. For segmentation, a lower scale

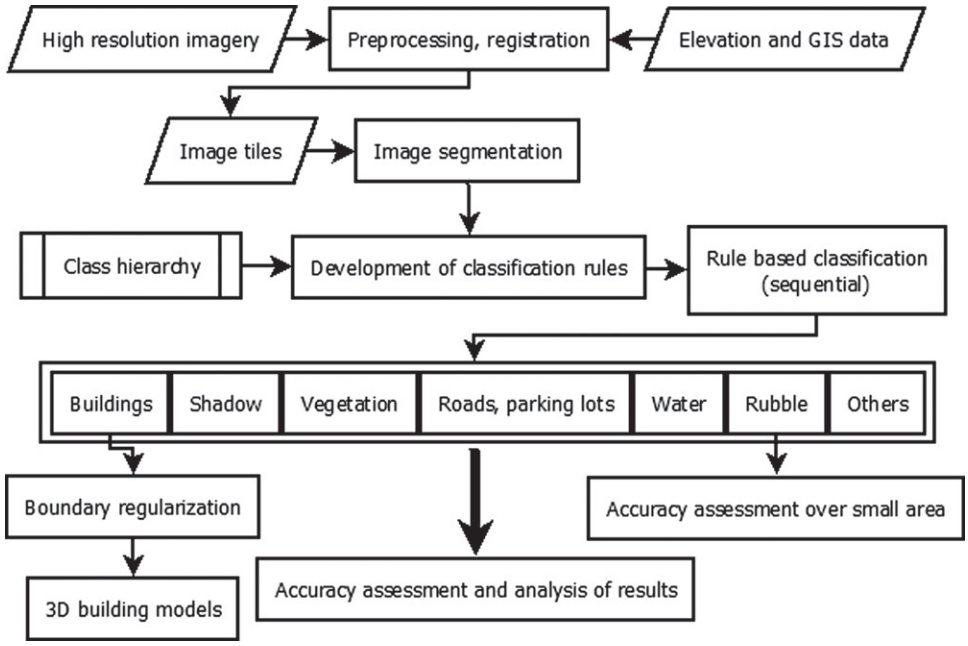

Figure 3. Flowchart of the processing scheme.

parameter was used in combination with higher spectral and shape parameters, to create meaningful, homogenous and compact objects which closely resemble buildings, the class of interest. After segmentation, spectral, shape, and texture features were calculated for each object, and appropriate class hierarchy was developed for classification. Classification was performed for seven land cover classes for this study area: (a) water, (b) vegetation, (c) shadow, (d) roads, streets, and parking lots, (e) buildings, (f) rubble, debris, and collapsed buildings, and (g) others. Class "others" includes mostly vehicles, temporary tents, and any other object left unclassified. Class "roads, streets, and parking lots" also includes the bare land patches, and the water class is mostly the sea water. Classification rules based on the combination of more informative and appropriate features that contribute significantly to a particular class were used to form classification rules. These features include spectral means and standard deviations of spectral bands, shape, and height. These rules are a set of conditions an object must meet to be assigned to a class. Classification was performed sequentially and iteratively, handling one class at a time, starting with the less confusing classes. Accordingly, classification results were checked at each stage for each class and rules were updated if required. A correctly classified class does not participate in the remaining classification process and acts as a mask. Such a sequential classification can be considered as hierarchical elimination of correctly classified classes from the remaining process. There is a lot of vegetation within and around the urban areas including trees and grasses. Since trees are not excluded from the DSM, it was necessary to classify vegetation first to exclude trees from further analysis so that the height information can be used for building classification. For this purpose, the Normalized Difference Green Red Vegetation Index (NDGRVI) was used (Walker and Blaschke, 2008).

Based on this method, a classification rule set was developed over a single tile image. Later, this rule set was transferred and applied to the remaining tile images for their classification. The transfer of the rule set to different image tiles required some modifications and updates to correctly classify objects having different characteristics than those for which the rule set was developed. However, the processing effort is significantly reduced since it helps to avoid repetitive training signatures selection for every other image, especially in the case of highly complex urban environments. All image tiles were classified accordingly and later combined to make one thematic map. A subset of the classified image showing the detailed level classification results such as a mapped single tree, a building and vehicles on the roads for part of the study area is shown in Figure 4. Also, the total area associated with each land cover class is given in Table 1.

Evaluation

To assess the accuracy of land cover classification, test samples for all land-cover classes were manually selected from the image. While selecting the test samples, it was ensured that they are true representatives of each relevant class, well dispersed over the image, and they include within class variations such as buildings with different types of roofs and the varying nature of building collapse and damage. Test samples, being the true representatives of considered land cover classes are expected to represent the classification accuracy accordingly. The confusion matrix showing different classification accuracy measures is given in Table 2.

Land cover classification performance with overall accuracy of 87 percent seems satisfactory considering the highly heterogeneous urban landscape of the study area. Classification accuracy was affected by several observable factors causing misclassification of the features in the study area.

Shadow from trees and buildings had very prominent dark response and was therefore easy to identify by using brightness means. However, there were confusions among the shadows and a few water features having very dark similar spectral response. Some of such areas have been

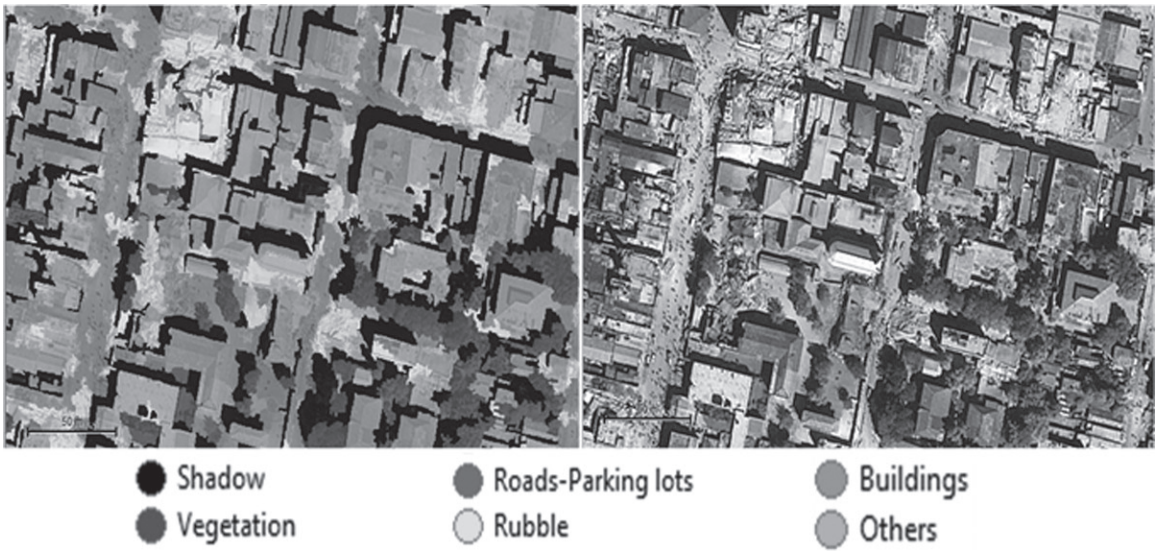

Figure 4. A subset of land cover image classification results

misclassified with each other. NDGRVI, and the ratio of green and blue bands classified most of the actual vegetation correctly even in the absence of near-infrared band. However, some of the buildings with green colored roofs were misclassified as vegetation. In such cases, even the use of texture, shape, and height information could not help to avoid this confusion. Green roof surfaces are very smooth and have well-defined rectangular shapes and height. Their texture and shape features resemble some of the grassy lawns outlined with walkways, and their heights are similar to the trees. These are very few such green color buildings, which were finally corrected and manually assigned to the building class.

Most of the undamaged concrete or metal sheet buildings are higher than five meters with different geometry, such as square, rectangular, and elongated. They also differ in their roof textures. Therefore, these buildings were classified into three sub-classes based on their height, shape, and texture features. Most of the shanty houses and shelters with metal sheet roofs are too low in height; therefore a minimum two meters height threshold was used for an object to be classified as a building. Using this method, almost every building which did not collapse has been correctly classified. Finally, sub-building classes were merged into a single building class.

Roads, streets, and parking lots are generally better classified. However, some of these have confusion with rubble since the streets next to concrete buildings are littered with building debris. Similarly, parked or moving vehicles are classified as others, rather than roads, streets, or parking lots. This confusion resulted in misclassification. "Others" class, being a combination of different objects has confusion with most of the other land cover classes; thus, resulted in lower classification accuracy.

TABLE 1. AREAS OF DIFFERENT LAND COVER CLASSES IN THE STUDY AREA

No	Land cover classes	Area (sq. km)
1	Water	6.57
2	Shadow	3.80
3	Vegetation	6.24
4	Roads, streets, parking lots, bare land	3.20
5	Rubble	2.00
6	Buildings	6.21
7	Others	0.95

TABLE 2. LAND COVER CLASSIFICATION ACCURACY BASED ON TEST SAMPLES (AFTER CONGALTON AND GREEN, 2009)

	Classified	Reference						
No	**Classes**	**1**	**2**	**3**	**4**	**5**	**6**	**7**
1	Water	**17013**	0	0	0	0	0	0
2	Shadow	355	**9611**	0	0	0	0	263
3	Vegetation	0	0	**16019**	0	0	713	0
4	Roads	0	0	0	**31051**	2037	0	437
5	Rubble	0	0	0	0	**15940**	0	4221
6	Buildings	0	0	0	0	13137	**52382**	292
7	Others	0	0	0	272	276	0	**3040**
	Sum	17368	9611	16019	31323	31390	53095	8253
	Producer Accuracy	0.98	1	1	0.99	0.51	0.98	0.37
	User accuracy	1	0.93	0.96	0.93	0.79	0.8	0.85
	Overall Accuracy		0.87		*Kappa*		0.833	

Building Extraction

The Buildings Class

Outcome from land cover mapping can be used to derive buildings. Building classification results are satisfactory for the urban areas where buildings are separated with well defined outlines and reasonable space between them (Figure 5a). Since the classification was based on the elevation, shape, and spectral characteristics of objects, classified building outlines follow the correct boundaries. However, at some places, classified building outlines include non-building objects having similar shape and spectral characteristics, or split the building outline in case of spectral variations within the building roofs. This results either in large size building outlines or a single building roof to split into more than one part (Figure 5c). However, after performing morphology operations and generalization, building outlines were improved, some of the extruding parts were removed, and holes were filled (Figure 5e). Another quality check was carried out over an area where the buildings are very closely spaced, crowded, different sizes, irregular layouts, and patterns (Figure 5b). In this case, almost all buildings have

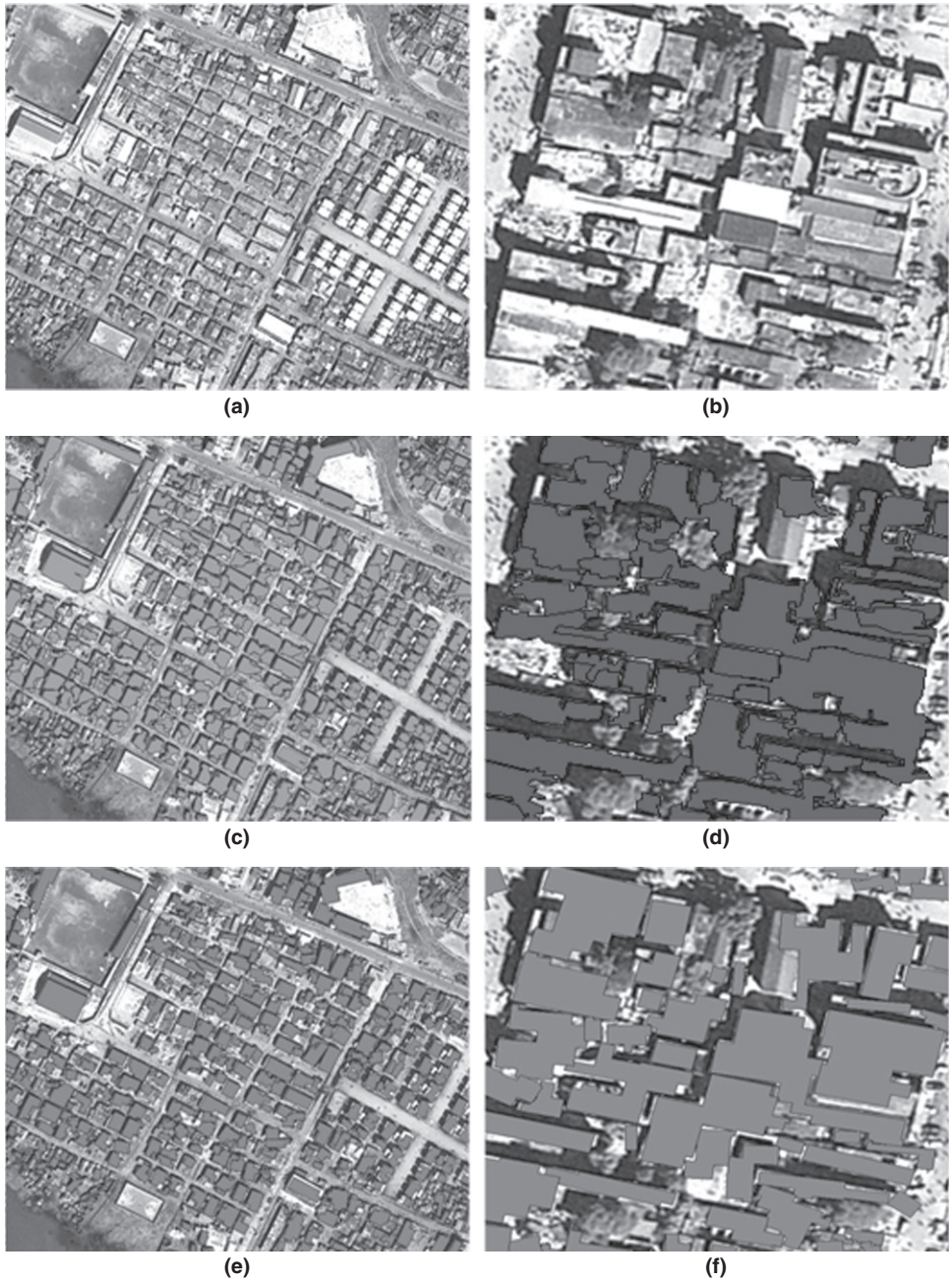

Figure 5. (a) a subset of GeoEye-1 image over an area with large and well separated buildings, (b) an area with irregular and closely spaced buildings; (a) and (b) original imagery, (c) and (d), extracted buildings, and (e) and (f) building outlines after necessary regularization.

been correctly identified except a part of a building roof with green color which has been classified in the "trees" class (Figure 5e). Due to spectral variations, a number of building roofs are split. Also, since the buildings within this area are very close or almost touching roofs, most of the close-by building outlines were merged to form large buildings with regularized outlines as shown in Figure 5f.

Regularization

The raster layer of extracted buildings obtained as a result of the land cover classification was converted to a vector polygon layer for further processing. Extracted building polygons were noisy and had irregular boundaries. A two-stage process was followed to simplify and regularize building boundaries. In the first stage, building polygons were checked and corrected for their geometry problems, such as self intersections and incorrect ring. Such issues may often be encountered during the initial establishment phase of a GIS database when data from different sources are required to be imported into the system. After repairing the geometry problems of the building polygons, small polygons which were parts of the buildings but fragmented during image classification were merged with the main building polygons, with which they shared an edge. Following this boundary improvement of defragmentation to some extent, they were also simplified by removing extra points close to each other. Though point removal both helped to reduce the data size and the workload of the building regularization algorithm, it also caused some problems regarding polygon topologies. Removal of points caused some of the neighboring or too close polygons to overlap with each other. Similar problems also occurred after building regularization and simplification process. Thus, such topology issues were fixed before and after applying the regularization algorithms.

Initial building boundaries are extracted from images as coarse approximations to the building outlines. They can be regarded as raw boundaries which comprise irregular edges as shown in Figure 6a. Regularization of these raw boundaries is necessary to retrieve and retain the main building shape. We apply constraints on the regularization based on commonly seen building styles to reduce the building shape complexity and the computation time. Most boundary edges are likely to be parallel to the dominant directions which are vectors representing the orientation of the building; moreover, most buildings tend to have two orthogonal dominant directions. Accordingly, the constraint is placed on the boundary edges such that they are forced to be parallel to the dominant directions (Fu and Shan, 2005). Sample results of building extraction (Figure 6a), simplification (Figure 6b), and regularization (Figure 6c) are presented in Figure 6.

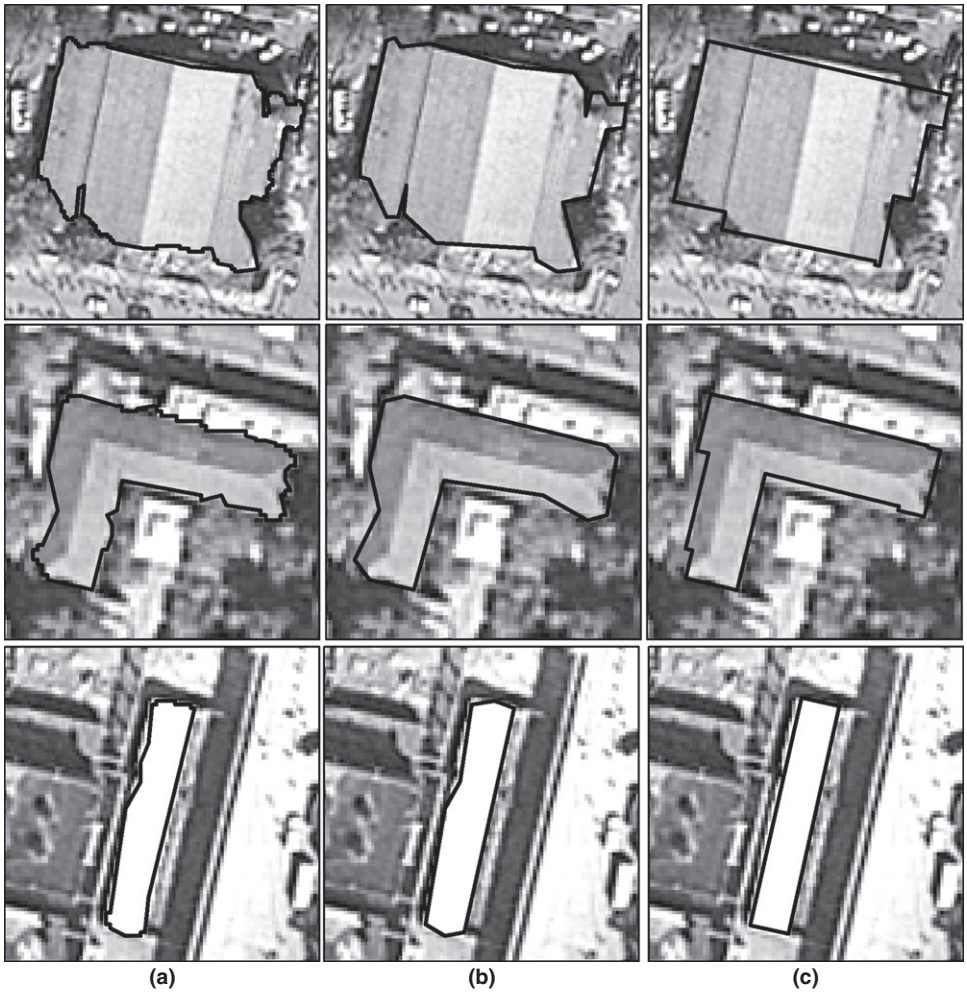

Figure 6. (a) sample results of building classification, (b) simplification, and (c) regularization.

3D Building Models

Generating 3D models of the buildings using various data sources, such as aerial images and lidar, provides an alternative way of interpretation of the urban structure by enabling different perspectives. Existing methods of 3D building model generation make use of the building footprints and roof shapes to generate a geometric representation of the buildings (Haala and Kada, 2010). Modeling complex structures is not an easy task and complete automation is also challenging (Habib *et al.*, 2010). Polyhedral models are commonly used for representing the building shapes by planar surfaces. Haala and Kada (2010) provide a recent overview of the state of the art on automatic 3D building reconstruction.

As discussed earlier, Port-au-Prince is a highly complex and heterogeneous urban area. Considering the complexity of the building structures within the study area and the concern for obtaining a rapid visual representation of the urban structure in the third dimension, we have adopted the basic box representation of the buildings using an average building height. Once regularized building outlines were obtained, their heights were calculated from the nDSM. Each building was assigned a height value that is one standard deviation higher than the mean of all the height values inside the building polygon. In some cases where more complex buildings with large height differences between their various parts (e.g., industrial buildings, buildings with towers, etc.) were extracted as a single polygon, it is observed that the assigned height values were not representing the actual height of the building. Distinct parts of such buildings were manually separated to represent their corresponding heights.

Following the assignment of height values to each individual building, extracted building footprints were extruded using the height information. Google SketchUp-6 plug-in for ArcGIS® is employed for generating the 3D models from building footprints. These 3D models were then exported to KMZ format. Providing 3D models in KMZ format using Google Earth is a very practical way of sharing such data for the communities of common interest. 3D models of approximately 55,000 buildings were generated as the end product, covering an area of 30 sq. km over Port-au-Prince. Figure 7 shows a subset of the GeoEye-1 image around the Presidential Palace, building footprints extracted from that image, 3D building models, and their draping over Google Earth imagery.

Rubble Mapping and Evaluation

The outcome of land cover mapping can also be used to access the distribution of rubble. Due to non-availability of pre-earthquake high-resolution image data at that time, cadastral information about the buildings, or building footprint data covering Port-au-Prince, it was hard to measure the accuracy of the mapped damaged buildings or rubble. However, one subset image covering approximately a 2 sq. km area with severely damaged buildings surrounding the Presidential Palace was used to estimate the rubble classification results. From this subset image, 200 ground truth test samples (polygon segments) of the actual damaged buildings were manually selected as shown in Figure 8. These damaged building test samples were then compared with the classification results of damaged buildings and rubble. This comparison shows that 190 damaged buildings out of 200 were completely or partly mapped, and 10 of them were misclassified and could not be mapped. Out of these 10 missed damage buildings, seven were either partly damaged or their roofs were collapsed, and they still had some significant height. The other three missed buildings are metal sheet roofs, parts of which were collapsed and parts were standing. Since texture and height were the main features used for rubble mapping, buildings with intact painted metal sheet roofs, as well as concrete based

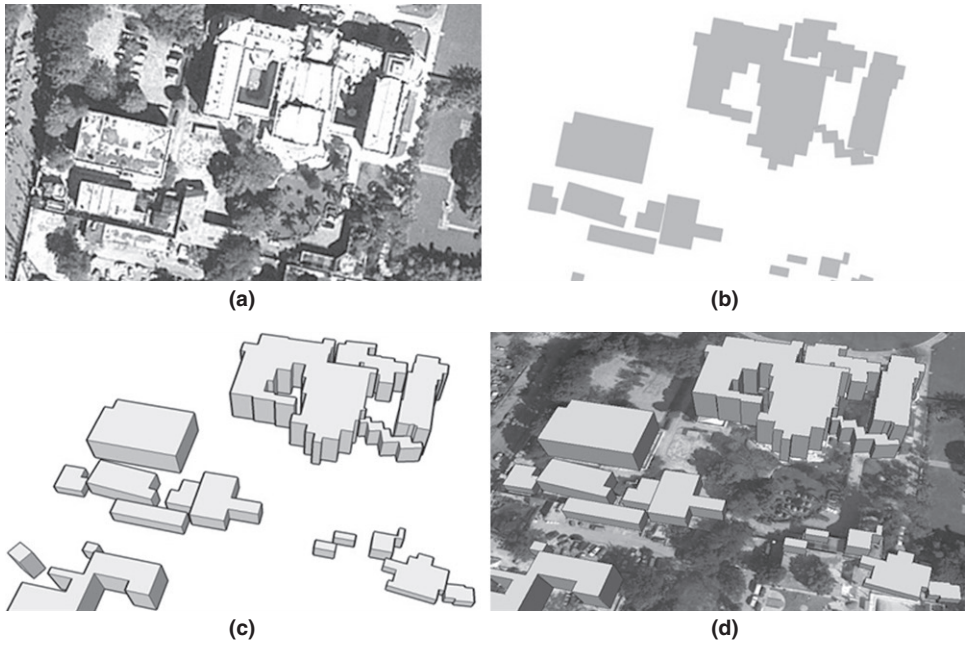

Figure 7. (a) subset of the GeoEye image around the Presidential Palace, (b) mapped building footprints, (c) 3D building models, and (d) 3D building models draped over a Google Earth image.

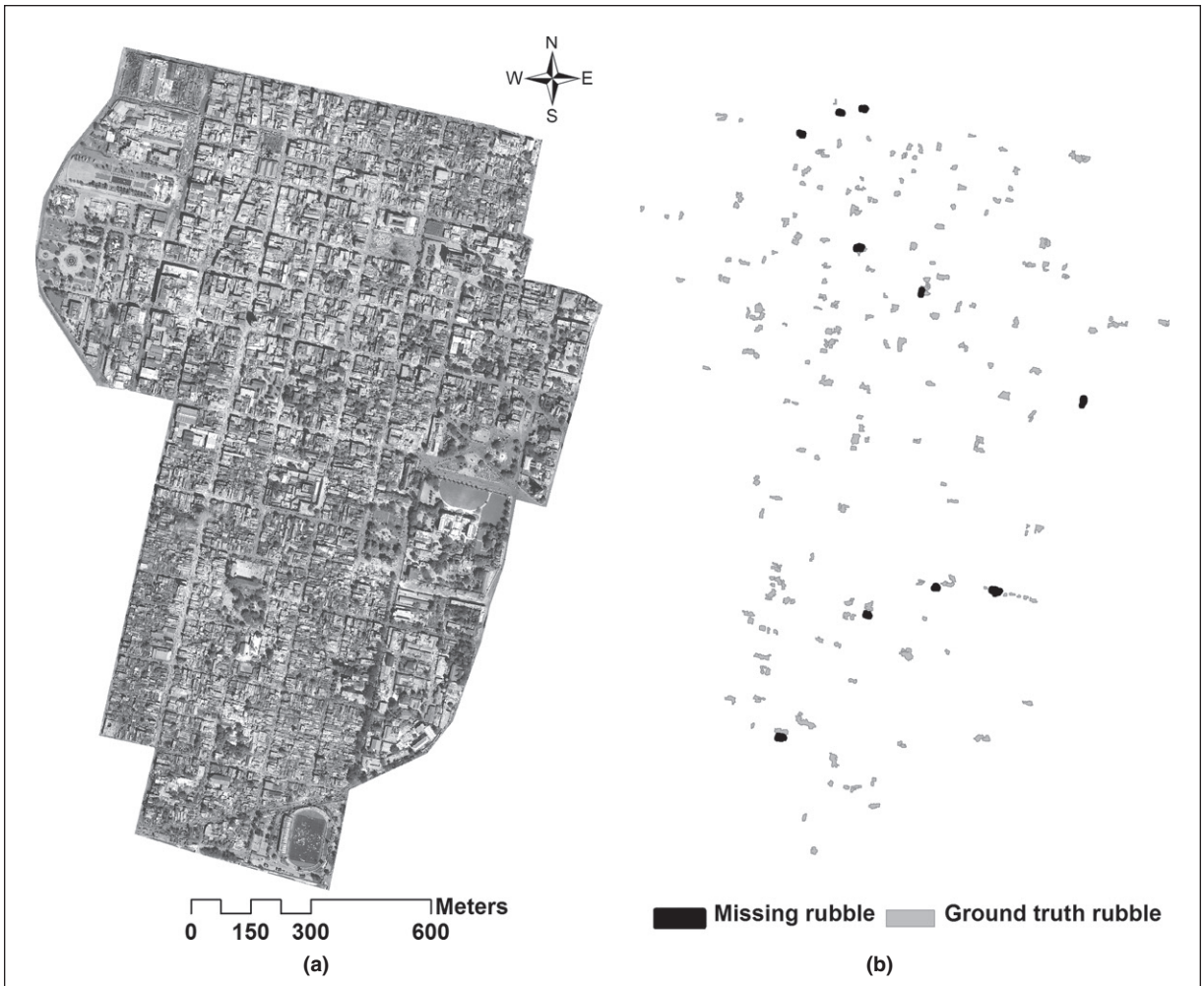

Figure 8. (a) the subset GeoEye-1 image used for rubble mapping and assessment, (b) rubble map (light tone for correctly identified rubble and dark tone for missed rubble).

collapsed buildings with unbroken roofs, could not be classified correctly. The quantitative results show that the damaged buildings within this 2 sq. km badly affected area created about 638,000 cubic meters of rubble and debris.

Due to the varying nature of building damage and collapse, some of the partially or totally collapsed buildings were classified as undamaged buildings. The reasons for such cases are various. For example, when building roof or a part of it is collapsed or caved in and its walls are still intact, such walls with any undamaged roof parts were classified as a building (Figure 9a). In some cases, a building's interior was partly classified as shadow because of the standing walls, and the broken parts not covered by shadow were classified as rubble. The standing parts of some of the partially damaged or collapsed buildings were classified as building due to their height and shape, but the broken parts were classified as rubble, e.g., the Presidential Palace (Figure 9b). When a multi-story concrete building with collapsed walls has an intact or partly collapsed roof with some height, it is hard to classify it as damaged or rubble. Such buildings were rather classified as undamaged buildings, and only the totally collapsed parts were classified as rubble (Figure 9c). Other examples of uncertainty and confusion in rubble mapping were steel or wooden frame buildings with metal sheet roofs, where the building was physically collapsed but there was no visible deformation or textural change to its roof structure except the broken concrete blocks or brick based side walls. Such buildings were hard to correctly classify as rubble unless their heights were lower than the height threshold. Buildings which just sat down with the whole roof either still intact or partly damaged were classified as undamaged and only their broken side walls were classified as rubble due to their distinct texture surface (Figure 9d). Such failures in the detection of damaged buildings which cause false negatives could potentially be minimized in case of pre-event lidar derived elevation data are available.

Concrete buildings have very prominent collapse or damage structures with totally broken down roofs and walls, thus were correctly classified as rubble due to their very distinct texture. There was negligible damage to metal sheet based shanty houses and shelters, except at places where roof sheets collapsed or were missing either previously or due to the earthquake. Such hollow roof shelters were classified as rubble. There were lots of debris spread over the roads and streets from the adjacent collapsed buildings and other dumped materials that were presumably recovered from collapsed buildings (Figure 9e). Such road and street segments are similar in spectral response and texture to rubble and debris, thus were classified as rubble. Shadows of the standing tall buildings on the adjacent collapsed buildings or on the roads and streets hindered rubble

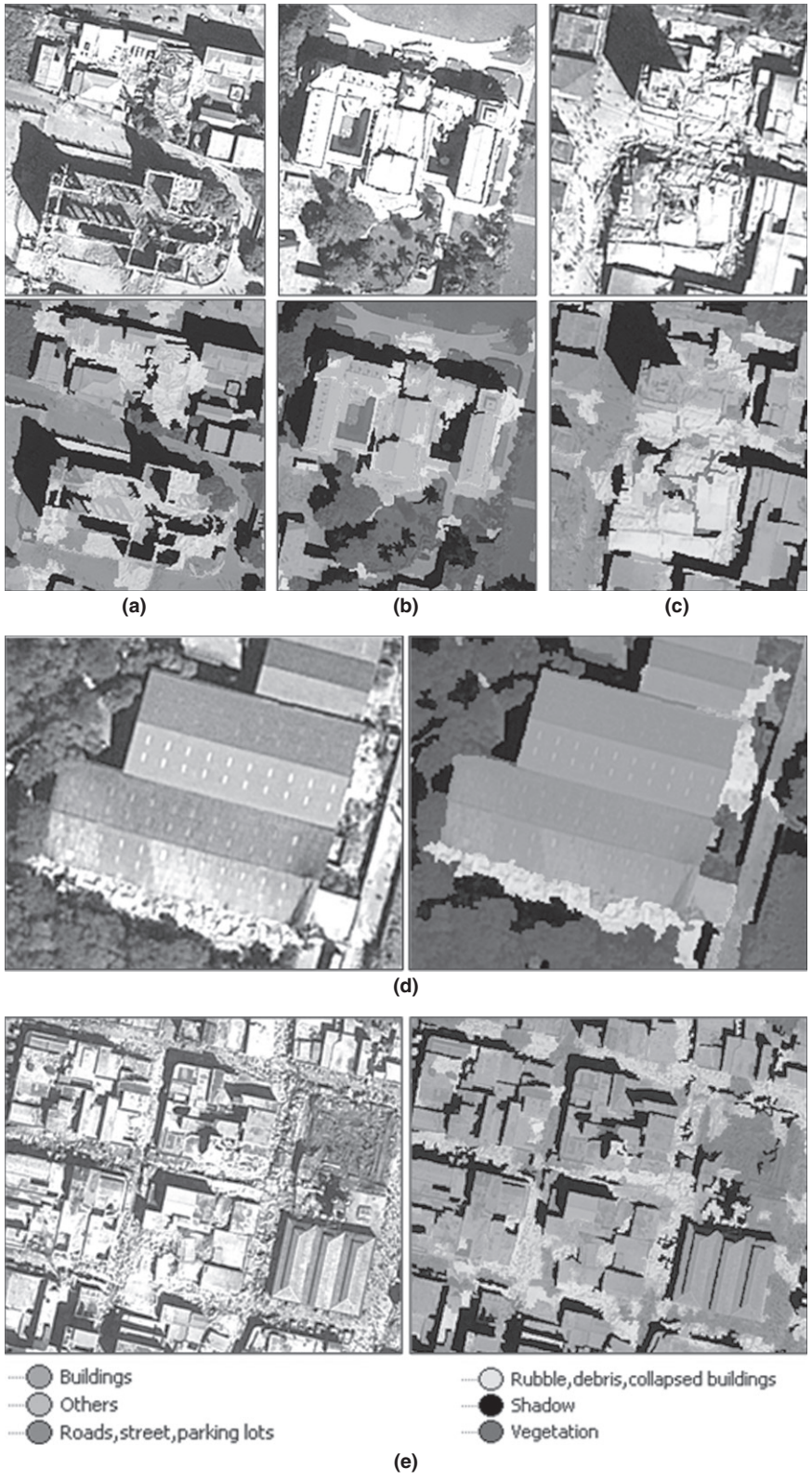

Figure 9. Examples of classification results of totally or partially damaged buildings, rubble and debris: (a) building roof partially collapsed with intact walls, (b) partially damaged building, (c) multi-story building with partially collapsed roof, (d) damaged building with intact roof, and (e) debris spread over roads and streets.

mapping. In this complex urban area, context to shadow could not be used to separate standing buildings from collapsed buildings. Even though a totally collapsed building did not cast any shadow, some of the partially collapsed buildings or their parts still had some shadow. Shadow size threshold did not work since the shadows caused by low height shanty houses are similar in size to the shadows cast by some of the partially collapsed buildings. At places, a large number of parked or dumped vehicles and other junkyards are similar in texture and spectral response; therefore they are classified as rubble and debris.

Post classification analysis indicates that the most affected buildings within Port-au-Prince are in the southwest of the Presidential Palace, a comparatively better planned area. Buildings in this area are mainly concrete constructions, i.e., reinforced concrete roofs with brick or concrete block walls. From an overall mapping of damage over the entire Port-au-Prince city, it was observed that concrete buildings were the worst affected, followed by wooden/steel frame metal roof buildings, and the least affected are shanty houses. Most of the concrete structures were badly damaged, broken down, and converted into rubble. Buildings with metal sheet roofs are mostly affected by the damaged side walls. The nature of the damage and patterns can be attributed to the poor construction quality, materials and construction practices. Some of the high rise buildings are still intact probably due to proper earthquake resistant design and construction. However, there seems to be either non-existence of or non-adherence to earthquake resistant building design and construction code. Due to the complexity of Port-au-Prince urban environment and non availability of pre-event high resolution data or existing building footprints, it is difficult to further categorize the types of building damage only based on remote sensing techniques.

Conclusions

Post-event GeoEye-1 imagery over Port-au-Prince proved to be one of the best data for urban area land cover mapping, especially for mapping urban features at fine scales. Land cover classification from imagery and nDSM combination produced satisfactory results with an overall accuracy of 87 percent. The Port-au-Prince urban area is very diverse and complex, with a large number of buildings of different types, sizes, density, texture, and height. This variety caused several problems during the classification process. In densely structured neighborhoods of the city, where tin roof, low height, and closely spaced dwellings with no visible edges exist, several buildings were aggregated as a single large building. Some of these could not be recognized as buildings due to very low heights and small areas. Similarly, some containers stored at the port were classified as buildings since they appeared similar in shape and height to buildings. Even with the above-mentioned problems, building extraction using object based classification from the combined image and nDSM produced satisfactory results for the entire GeoEye-1 image, covering a large area in which about 55,000 buildings were mapped. Due to no specific shape, pattern, and spectral response, it was extremely hard to classify the rubble. Similarities in the spectral responses, shapes and heights of buildings and other debris or junkyards resulted in confusion and misclassification of class "rubble" with classes "buildings" and "others" with producer and user accuracies of 51 percent and 79 percent, respectively.

During the classification, almost all of the buildings were picked up to their fine level, but their non-crisp outlines required regularization for improvement. Building regularization needs very extensive effort; it overestimates, removes some actual building parts, and in some cases even distorts building positions. These regularized 2D buildings produced reasonably good quality models once converted to 3D building models which are very helpful to visualize actual city structure and landscape.

The use of optical high-resolution satellite remote sensing image data proved very helpful for mapping the damage, its nature and extent during the recent Haiti earthquake. The availability and use of VHR imagery augmented with ancillary lidar based elevation information can help mapping very fine scale disaster damage severity and its impact within the urban areas. Elevation derived from lidar provides important aid in determining damaged buildings by introducing the missing dimension in the remote sensing imagery. However, failures in the detection of damaged buildings still exist; especially for "pancake" type of damaged buildings. If available, including the pre-event lidar data in the process may help minimize this problem. The analysis indicates higher rate of damage to concrete and masonry structures compared to other types of construction. Typical nature and pattern of damage to concrete buildings include total destruction, partial collapse, and collapse of the columns and walls. Damage to masonry structures is not restricted to any particular area; rather they occurred wherever such construction exits in Port-au-Prince. In most of the places, steel and wooden frame structures are collapsed and partially damaged due to the failure of supporting masonry walls or columns. Shanty houses are least affected by the earthquake activity. The severity of the structural damage to all types of buildings can also be attributed to poor quality construction, non-existence or adherence to earthquake resistant building designs, and the economical conditions of the people, as well as the country.

An accurate damage assessment is only possible through field surveys. However, it requires extensive time and substantial resources. This study attempted to use remote sensing data to obtain a relatively quick preliminary overview of the damage after the earthquake in Port-au-Prince, a city with very complex urban structure. The outcome shows that remote sensing data can be a potential source for preliminary damage and rubble mapping in similar situations. Preliminary damage estimates from remote sensing data can help to make movement plans to locate and to reach the target areas. At the later stages it can be used to assess the volume of the rubble and debris, to plan and prioritize efforts and resources required for clearance.

References

Ali, S.T., A.M. Freed, E. Calais, D.M. Manaker, and W.R. McCann, 2008. Coulomb stress evolution in Northeastern Caribbean over the past 250 years due to coseismic, postseismic and interseismic deformation, *Geophysical Journal International*, 174:904–918.

Baatz, M., and A. Schäpe, 2000. Multiresolution segmentation - An optimization approach for high quality multi-scale image segmentation, *Angewandte Geographische Informationsverarbeitung XII, Beiträge zum AGIT-Symposium Salzburg* (J. Strobl, T. Blaschke, and G. Griesebner, editors), Herbert Wichmann Verlag, Karlsruhe, pp. 12–23.

Benz, U.C., P. Hofmann, G. Willhauck, I. Lingenfelder, and M. Heynen, 2004. Multi-resolution, object-oriented fuzzy analysis of remote sensing data for GIS ready information, *ISPRS Journal of Photogrammetry and Remote Sensing*, 58:239–258.

Chen, Y., P. Shi, T. Fung, J. Wang, and X. Li, 2007. Object-oriented classification for urban land cover mapping with ASTER imagery, *International Journal of Remote Sensing*, 29:4645–4651.

Eberhard, M.O., S. Baldridge, J. Marshall, W. Mooney, and G.J. Rix, 2010. *The M_W 7.0 Haiti Earthquake of January 12, 2010: USGS/EERI Advance Reconnaissance Team Report,* U.S. Geological Survey Open-File Report 2010–1048, URL: *http://pubs.usgs.gov/of/2010/1048/* (last date accessed: 06 July 2011)

Fu, C., and J. Shan, 2005. Construct 3D building topology based on point primitives, *Proceedings of the 8th International Conference on GeoComputation,* 31 July - 03 August Ann Arbor, Michigan, unpaginated CD-ROM.

Geofabrik, 2010.URL: *http://www.geofabrik.de/data/download.html* (last date accessed: 06 July 2011).

Gusella, L., B.J. Adams, G. Bitelli, C.K. Huyck, and A. Mognol, 2005. Object-oriented image understanding and post-earthquake damage assessment for the 2003 Bam, Iran, Earthquake, *Earthquake Spectra*, 21(S1):225–238.

Haala, N., and M. Kada, 2010. An update on automatic 3D building reconstruction, *ISPRS Journal of Photogrammetry and Remote Sensing*, 65:570–580.

Habib, A.F., R. Zhai, and C. Kim, 2010. Generation of complex polyhedral building models by integrating stereo-aerial imagery and lidar data, *Photogrammetric Engineering & Remote Sensing*, 76(5):609–623.

Hay, G.J., T. Blaschke, D.J. Marceau, and A. Bouchard, 2003. A comparison of three image-object methods for the multiscale analysis of landscape structure, *ISPRS Journal of Photogrammetry and Remote Sensing*, 57(5-6):327–345.

Myint, S.W., M. Yuan, R.S. Cerveny, and C. Giri, 2008. Categorizing natural disaster damage assessment using satellite-based geospatial techniques, *Natural Hazards Earth System Sciences*, 8(4):707–719.

O'Loughlin, K.F., and J.F. Lander, 2003. *Caribbean Tsunamis, A 500-Year History from 1498-1998*, Kluwer Academic Publishers, The Netherlands, 263 p.

Platt, R.V., and L. Rapoza, 2008. An evaluation of an object-oriented paradigm for land use/land cover classification, *The Professional Geographer*, 60(1):87–100.

Rathje, E.M., M. Crawford, K. Woo, and A. Neuenschwander, 2005, Damage patterns from satellite images from the 2003 Bam, Iran Earthquake, *Earthquake Spectra*, 21(S1):295–307.

Scherer, J., 1912. Great earthquakes in the Island of Haiti, *Bulletin of the Seismological Society of America*, 2(3):161-180.

Shackelford, K., and C.H. Davis 2003. A hierarchical fuzzy classification approach for high-resolution multispectral data over urban areas, *IEEE Transactions on Geoscience and Remote Sensing*, 41(9):1920–1932.

Shan, J., and E. Hussain, 2010. Object-based data integration and classification for high-resolution coastal mapping, *Remote Sensing of Coastal Environments* (Y. Wang, editor), CRC Press, Taylor & Francis Group, Boca Raton, Florida, pp. 210–234.

Shan, J., E. Hussain, K. Kim, and L. Biehl, 2010. Flood mapping with satellite images and its web service, *Photogrammetric Engineering & Remote Sensing*, 76(2):102–105.

Stryker, T., and B. Jones, 2009. Disaster response and the international charter program, *Photogrammetric Engineering & Remote Sensing*, 75(12):1342–1344.

Turker, M., and B. Cetinkaya, 2005. Automatic detection of earthquake-damaged buildings using DEMs created from pre- and post-earthquake stereo aerial photographs, *International Journal of Remote Sensing*, 26:823–832.

Turker, M., and E. Sumer, 2008. Building-based damage detection due to earthquake using the watershed segmentation of the post-event aerial images, *International Journal of Remote Sensing*, 29(11):3073–3089.

van der Sande, C.J., S.M. de Jong, and A.P.J. de Roo, 2003. A segmentation and classification approach of IKONOS-2 imagery for land cover mapping to assist flood risk and flood damage assessment, *International Journal of Applied Earth Observation and Geoinformation*, 4(3):217–229.

Walker, J.S., and T. Blaschke, 2008. Object-based land-cover classification for the Phoenix metropolitan area: Optimization vs. transportability, *International Journal of Remote Sensing*, 29(7):2021–2040.

Yamazaki, F., Y. Yano, M. Matsuoka, 2005. Visual damage interpretation of buildings in Bam City using QuickBird images following the 2003 Bam, Iran, Earthquake, *Earthquake Spectra*, 21(S1):329–336.